# **Bi**@hemistry

pubs.acs.org/biochemistry Article

### Putative Pore Structures of Amyloid $\beta$ 25–35 in Lipid Bilayers

Ankita Dutta, Aliasghar Sepehri, and Themis Lazaridis\*



Cite This: Biochemistry 2023, 62, 2549-2558



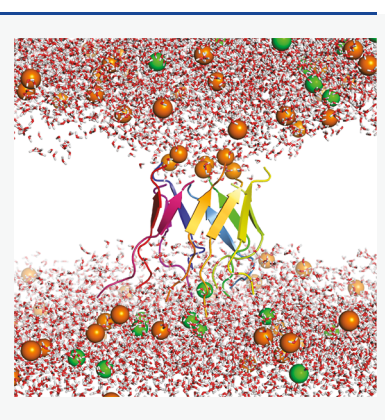
**ACCESS** 

Metrics & More

Article Recommendations

Supporting Information

**ABSTRACT:** The amyloid β peptide aggregates to form extracellular plaques in the brains of Alzheimer's disease patients. Certain of its fragments have been found to have similar properties to those of the full-length peptide. The best-studied of these is 25-35, which aggregates into fibrils, is toxic to neurons, and forms ion channels in synthetic lipid bilayers. Here, we investigate possible pore-forming structures of oligomers of this peptide in a POPC/POPG membrane. We consider octameric and decameric β-barrels of different topology, strand orientation, and shear, evaluate their stability in an implicit membrane model, and subject the best models to multimicrosecond all-atom molecular dynamics simulations. We find two decameric structures that are kinetically stable in membranes on this time scale: an imperfectly closed antiparallel β-barrel with K28 in the pore lumen and a short parallel β-barrel with K28 toward the membrane interface. Both structures exhibit dehydrated gaps in the pore lumen, which are larger for the antiparallel barrel. Based on these results, the experimental cation selectivity, the dependence of ion channel activity on voltage direction, and certain mutation data, the parallel model seems more compatible with experimental data.



#### **■ INTRODUCTION**

The amyloid  $\beta$  (Ab) peptide, produced by enzymatic cleavage of the amyloid precursor protein, is the main constituent of the senile plaques that characterize Alzheimer's disease. The most common forms of the peptide are Ab1-40 and Ab1-42, but shorter fragments also occur naturally and have been studied in vitro. One fragment that received considerable attention is Ab25-35, the shortest fragment that retains important physical and biological activities of the full-length peptide.<sup>2,3</sup> For example, it aggregates into fibrils, 4,5 potentiates disruption of Ca<sup>2+</sup> homeostasis by excitatory amino acids,<sup>6</sup> increases ion conductance<sup>7,8</sup> and membrane permeability<sup>9</sup> in neurons, triggers apoptosis,<sup>5,10,11</sup> and causes cell lysis in RBCs.<sup>12</sup> One study found Ab25-35 in Alzheimer's patients' brains 13 although it is not one of the major species. 14-16 In vitro experiments showed that this fragment can form ion channels in planar membranes<sup>17,18</sup> and cause Ca<sup>2+</sup> influx<sup>19</sup> and dye leakage<sup>20</sup> in vesicles, providing a possible mechanism of cytotoxicity.

The C-terminal half of Ab25-35 is hydrophobic and interacts readily with membranes, preferably anionic due to  $K28^{21}$  but also purely zwitterionic. <sup>22,23</sup> Small angle X-ray diffraction <sup>22</sup> and neutron diffraction <sup>23,24</sup> showed this peptide integrating into the hydrophobic acyl chain region of the lipid bilayer and causing disruption of the membrane structure. EPR experiments in SUVs showed the C-terminal half to be ordered and inserted into the membrane, while the N-terminal end remains disordered in solution. <sup>25</sup> Cholesterol causes ordering of the lipid phase and thereby hampers the insertion of  $A\beta$  peptides into the membrane bilayer <sup>18,26,27</sup> but has a more complex effect on pore formation. <sup>20</sup> The structure of the peptide in micelles and

nonpolar solvents is helical, ^25,28,29 but  $\beta$  conformation has been found in aqueous solution. <sup>19,30,31</sup>

Ab25-35 has been the subject of several computational studies. Replica exchange in water and water/HFIP reproduced the preference for helix in apolar solvents and  $\beta$  structure in water<sup>32</sup> and showed partial helix formation in implicit membranes.<sup>33,34</sup> Replica exchange with solute tempering in explicit bilayers showed a partially helical peptide which inserts deeper when it forms dimers.<sup>35–37</sup> A hypothetical model for a large pore created by the propagation of the observed interactions was also proposed.<sup>36</sup> The possibility of  $\beta$ -barrel formation was also examined around nanotubes<sup>38</sup> and in lipid bilayers.<sup>39</sup> In the latter work, six  $\beta$ -barrels were considered and one was found to remain inserted and hydrated on the 150 ns time scale.

Despite the substantial experimental and computational work, the structure of membrane pores created by A $\beta$ 25-35 remains elusive. In the work presented here, a large number of theoretical models of  $\beta$ -barrels formed by A $\beta$ 25-35 were generated and evaluated first using molecular dynamics (MD) simulations in implicit membranes. The most stable models were then embedded into an all-atom POPC/POPG bilayer and subjected to long-time-scale MD simulation in order to assess their stability and the lipid—protein interactions that stabilize them.

Received: June 22, 2023 Revised: July 31, 2023 Published: August 15, 2023





#### METHODS

Model Construction and Evaluation in Implicit **Solvent.** The amino acid sequence of A $\beta$ 25-35 is GSNKGAIIGLM. Within this sequence, two motifs, GAIIGL and AIIGLM, produce antiparallel and parallel  $\beta$  sheets, respectively, in microcrystal structures. Therefore, we generated both parallel and antiparallel  $\beta$ -barrels de novo. A single  $A\beta$  peptide strand was first replicated and translated laterally to form a parallel dimer. The replicated strand was rotated appropriately to create antiparallel dimers. A flat oligomer was then constructed by replicating and translating laterally each A $\beta$ 25-35 dimer. This procedure generates unsheared barrels. Two levels of shear were then introduced: "full shear", by translating each peptide up or down along its axis so that the H-bonding register shifts by one, and "half shear", where every other peptide is thus shifted. The direction of this shift determines the tilt sense of the strands in the final barrel structure and the orientation of the strands with respect to the barrel interior.

Following the construction of a flat oligomer, distance restraints were added between H bonding pairs in all strands except for the ones at the ends. The oligomer was subjected to a short MD run in EEF1 effective energy function followed by energy minimization. EEF1 is a combination of the CHARMM 19 united atom force field with a Gaussian solvent-exclusion solvation free energy term. At the conclusion of this step, a natural curvature develops for the sheared barrels that either placed the Lys28 facing into the barrel (K-in) or out of the barrel (K-out). Further distance restraints were then applied to the end strands to enforce barrel closure. Initially eight-stranded parallel and antiparallel  $\beta$ -barrels were created using the method described, based on available data. <sup>19,20</sup> Because these appeared too tightly packed, 10-stranded barrels were also constructed.

The newly constructed  $\beta$ -barrels were then aligned along the z-axis and inserted into IMM1 implicit membrane pores.  $^{43-45}$  IMM1 is an extension of EEF1 to heterogeneous membrane-water systems. It models the membrane as a hydrophobic slab and uses a switching function that transitions smoothly from a nonpolar to an aqueous environment. The headgroup area is not distinguished from the aqueous region, so specific interactions with the lipid headgroups are ignored. Only the headgroup charge is taken into account with the Gouy—Chapman model (not used here). Modeling of pores is accomplished by making the switching function F dependent on not only the vertical (z) coordinate but also the distance r from the z-axis (see eq 1).

$$\begin{split} F(z', \, r') &= f(z') + b(r') \, - f(z') b(r'), \\ f(z') &= \frac{z'^n}{1 + z'^n}, \qquad b(r') = 1 \, - \frac{r'^n}{1 + r'^n} \\ z' &= |z|/(T/2), \qquad r' = r/R, \qquad R = R_o + kz'^2 \end{split}$$

T= membrane thickness. The z-axis is perpendicular to the membrane at the pore center.

The shape of the pore was toroidal with k=10, and the radius  $R_{\rm o}$  was set based on the position of the peptide backbone (9.5 Å for the 10-mers). The CHARMM software package was used for classical MD simulations. <sup>47</sup> The  $\beta$ -barrels were subjected to MD runs in implicit membrane pores for 100 ps, followed by further minimization. The final energy was compared to the energy of the same structure in water to obtain the  $\Delta W$  of transfer. The structures with the most favorable  $\Delta W$  were chosen for further

study using all-atom simulation. This transfer energy is a quick estimate of the favorability of membrane insertion and is dominated by the intermolecular interactions of the peptide with lipids and water (hydrophobicity and polar desolvation). It is not the full free energy of binding as it ignores peptide entropy effects, conformational changes from water to membrane, and the free energy of deforming the membrane into the selected shape. It thus gives only a partial measure of the stability of a peptide-stabilized membrane pore. The negative value of this quantity is a necessary but not sufficient condition for favorable membrane insertion. Our lab has used this implicit membrane pore approach to study antimicrobial peptides,  $^{45,48-50}$  protegrin,  $^{51-54}$  and recently putative pore structures formed by amylin,  $^{55}$  full-length Ab42,  $^{56}$  and  $\alpha$ -synuclein.  $^{57}$  All-Atom Simulations. Two  $\beta$ -barrels that had the most

stability and favorable transfer energy in implicit membrane pores were chosen for all-atom simulations. They were first placed along the z-axis, perpendicular to the membrane. The structures were then uploaded to the CHARMM-GUI server, where 300 lipids and a water slab with a thickness of at least 17.5 Å were added. The membrane consisted of 75% POPC and 25%  $\,$ POPG (240 POPC and 60 POPG lipids). This mixture is typical for in vitro liposome experiments and has been used to study membrane binding by Ab25-35 peptides.<sup>21</sup> The charmm36 force field was used for the peptide<sup>58</sup> and the lipids,<sup>59</sup> and the TIP3P model was used for water. Potassium chloride (0.15 M) was added, with extra K<sup>+</sup> ions to neutralize the excess negative charge of the peptide-lipid system. The parallel 10-mer system contained 10,742 waters, 77 K<sup>+</sup>, and 27 Cl<sup>-</sup>, and the antiparallel system contained 10,710 waters, 72 K<sup>+</sup>, and 22 Cl<sup>-</sup>. The systems were first equilibrated locally using NAMD software as described in previous work.<sup>55</sup> The final structures after equilibration were subjected to 10  $\mu s$  simulations on the ANTON2 supercomputer.<sup>60</sup>

#### RESULTS

Model Construction and Evaluation in Implicit Solvent. The barrels constructed here can be classified according to four attributes: (a) parallel or antiparallel, according to the direction of neighboring strands, (b) K-in or K-out, according to strand orientation with respect to the pore, (c) unsheared, full-sheared, or half-sheared, according to the amount of shear, and (d) 8-mers or 10-mers, according to the oligomeric state. Parallel barrels place all the Lys close to each other, which should be electrostatically unfavorable. Antiparallel barrels place the Lys at two different heights, which is preferable in terms of interpeptide interactions but may be unfavorable in terms of peptide-lipid interactions (see below). The shear affects the ability of the peptide to span the bilayer. Unsheared barrels are the longest but are inherently unstable, 51 so they are not considered here. Full-sheared barrels span about half the membrane, and half-sheared barrels span about 3/4 of the membrane. The oligomeric state affects the size of the pore. 8mers are very tight with little empty space in the pore, whereas 10-mers are more loosely packed.

Table 1 shows the transfer energy of selected models from water to an implicit membrane pore. Antiparallel K-out 8-mers were the least stable and partially moved out of the membrane. In these structures, it is difficult for the Lys to avoid the nonpolar membrane environment. K-in antiparallel 8-mers are also not very stable. The half-shear barrel breaks, whereas the full-shear barrel remains intact but spans only half of the membrane. In the parallel K-out barrels, all the Lys are at the same height, so the

Table 1. Transfer Energies ( $\Delta W$ ) from Water to Implicit Membrane Pores of Different  $\beta$ -Barrel Models (kcal/mol)<sup>a</sup>

	K-in	K-out	K-in	K-out
	parallel 8-mers		antiparallel 8-mers	
half shear	-11.6	-36	5.1	(-2.6)
full shear	-2.1	-30	9.4	(0.0)
	parallel 10-mers		antiparallel 10-mers	
half shear	-6.3	-46	0.6	11.5
full shear	-0.2	-29	29.5	2.3

<sup>&</sup>lt;sup>a</sup>Parentheses signify that the peptide complex left the membrane pore.

barrel can move to one side of the membrane to allow them to interact with the polar phase. Because of that, the transfer energies are very favorable. We should keep in mind, though, that these energies do not include the free energy of deforming the membrane, so they overstate the pore's stability. Leaving some of the pore uncovered by peptides costs considerable free energy that would lower the favorability of these structures. Parallel K-in barrels pack the Lys close to each other. As a result, the half-shear barrel breaks at a single point. The full-shear K-in parallel barrel remains intact but is marginally favorable.

Because of the very tight side chain packing of 8-mers, we considered slightly larger structures made of 10-mers. The trends here are similar to those with 8-mers, but no break in the barrel occurs in half-shear parallel and antiparallel K-in barrels. The transfer energy of the antiparallel K-in 10-mer is now close

to zero, while the parallel K-out 10-mer shows an even more favorable  $\Delta W$ . Based on the transfer energies and the integrity of the barrels, we chose to subject two 10-mer barrels to all-atom simulations: the half-shear parallel K-out (P10Kout) and the antiparallel K-in (A10Kin) (Figure 1).

All-Atom Simulations. The two selected half-shear decameric  $\beta$ -barrels were subjected to all-atom MD simulation to ascertain their stability in explicit membranes. The structures were 27–30 Å in length, enough to span the hydrophobic core of the lipid bilayer. The  $\beta$ -barrels were therefore fully embedded into the membrane and simulated for 10  $\mu$ s. At the end of these simulations, both structures remained in the membrane. The Nterminal region of the P10Kout structure, which extended beyond the lipid bilayer and into the water slab, assumed a disordered structure producing an unfurled funnel-like end to a short cylindrical barrel (Figure 2). The K28 side chains are at the level of the lipid phosphates and interact frequently with them. Although they are all oriented outward in the initial structure, the disordering of the N-terminal region allows some of them to flip inward (top views in Figure 2). RMS deviation as a function of time, secondary structure propensity for each residue, contact maps, H bonds involving K28, and K28-phosphate contacts are shown in Figures S1, S3, S5, S8a, and S9a in the Supporting Information, respectively.

The A10Kin structure produced a more compact cylindrical barrel that retained its initial structure more closely (Figure 3). However, a shift in register and then a break developed between

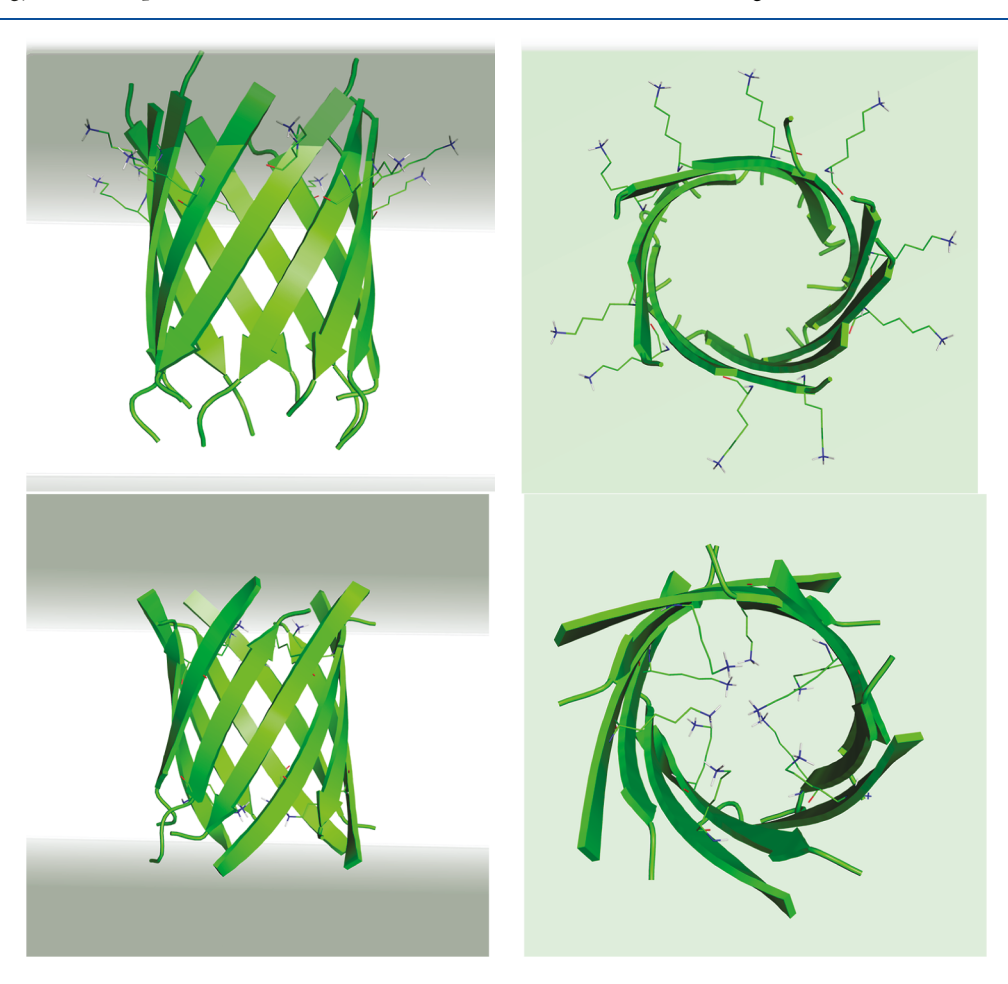


Figure 1. Parallel Kout 10-mer (top) and antiparallel Kin 10-mer (bottom), side (left) and top (right) views. The gray area signifies the aqueous environment. The K28 residues are shown as sticks.

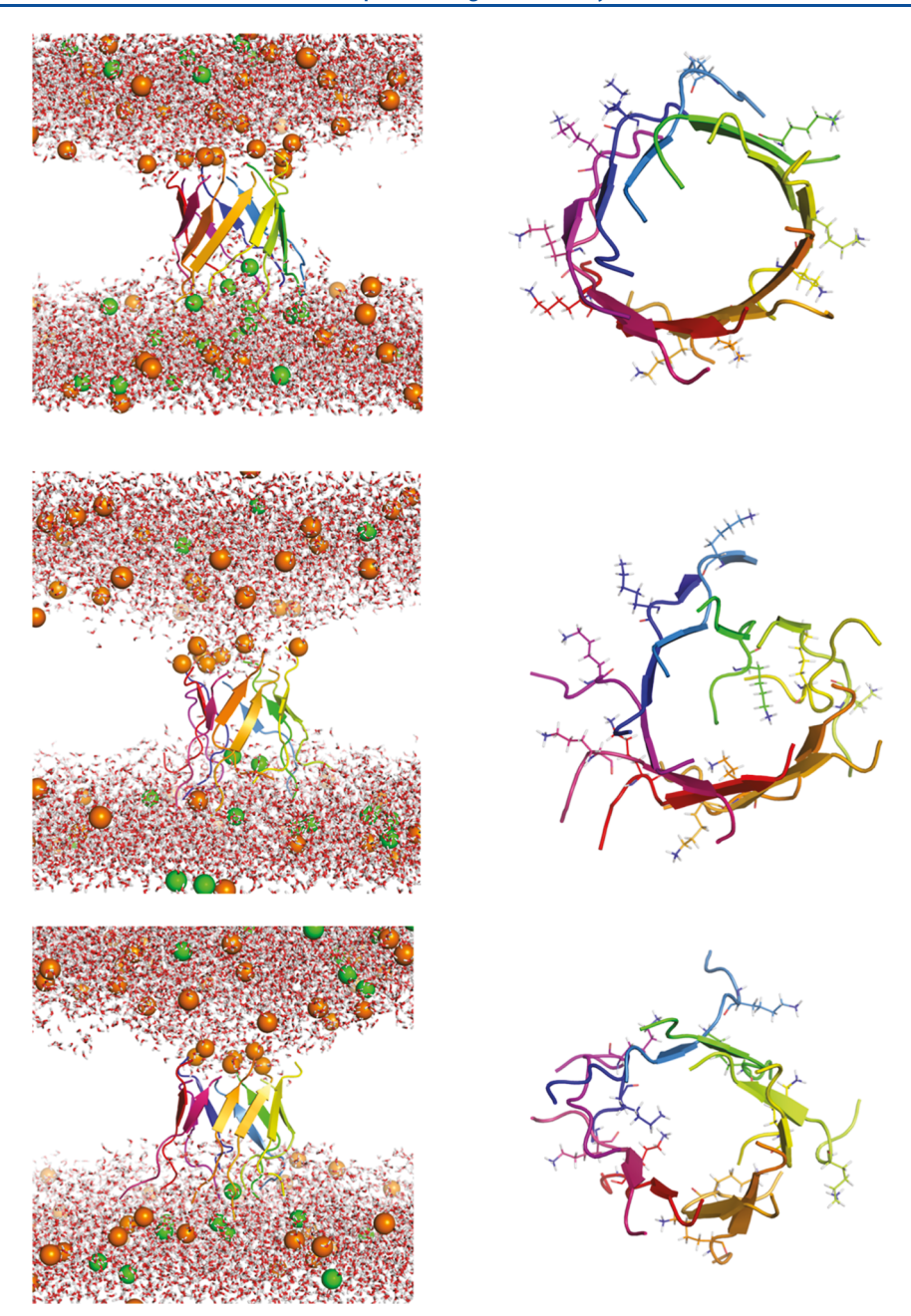


Figure 2. P10Kout at the start of the simulation (top), after 5  $\mu$ s (middle) and after 10  $\mu$ s (bottom). Left panel: side view; right panel: top view. The lipids are not shown for clarity. The green spheres are chloride ions, and the orange spheres are potassium ions. K28 side chains are shown in the top view.

two monomers (depicted using light blue and deep blue  $\beta$ -strands in Figure 3). The C-terminal end of the light blue monomer entered the pore lumen, first around 500 ns, apparently to interact with a lysine. An increase in the average distance between the two monomers is noticeable around 7.5  $\mu$ s, from 5–7 to 8–10 Å. No H bonding exists between them at the end of the simulation. In spite of this, the average diameter (backbone to backbone) at the center of the pore remains ~19 Å throughout the trajectory. The K28 side chains are all oriented inward in the initial structure, but the repulsion between them forces some to move out of the pore lumen (top views in Figure 3). RMS deviation as a function of time, secondary structure propensity for each residue, contact maps, H bonds involving K28, and K28-phosphate contacts are shown in Figures S2, S4, S6, S7, S8b, and S9b in the Supporting Information, respectively.

Analysis of Energetics. To gain insights into the factors that affect the stability of these barrels, the trajectories were analyzed to obtain interaction energies of the peptides with themselves and with the lipids (Table 2). The peptide—lipid energy contributions were normalized by the number of lipids present. We find that, on average, protein—POPG interaction per molecule of POPG is stronger than protein—POPC interaction per molecule of POPC. This is true for both barrels and is likely due to the fact that POPG has a net charge of —1. The positively charged Lys28, which tends to localize at the membrane interface, accounts for about half of this difference (the N-terminus also contributes significantly to this difference, whereas polar residues such as Ser and Asn interact slightly more strongly with POPG). The K28lipid interactions are weaker for

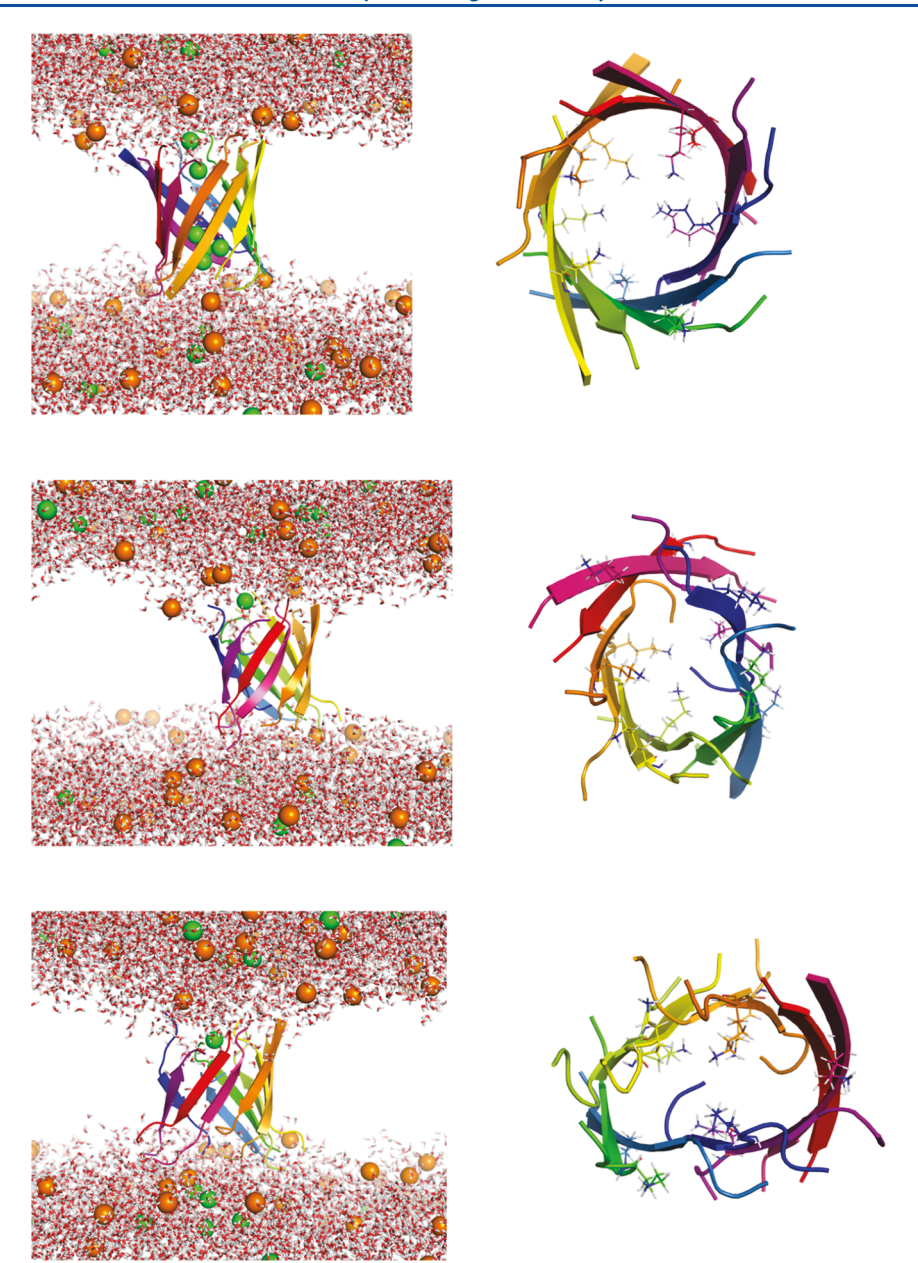


Figure 3. A10Kin at the start of the simulation (top), after  $5 \mu s$  (middle) and after  $10 \mu s$  (bottom). Left panel: side view; right panel: top view. K28 side chains are shown in the top view. Colors are the same as those in Figure 2.

Table 2. Protein-Lipid and Interpeptide Interaction Energy (kcal/mol)<sup>a</sup>

system	protein-POPC (K28-POPC)		protein—POPG (K28-POPG)		interpeptide	
	first 2 μs	8–10 μs	first 2 μs	8–10 μs	first 2 μs	8–10 μs
P10Kout energy/lipid	$-656 \pm 130 \ (-217 \pm 83)$ $-2.73 \ (-0.90)$	$-708 \pm 125 (-250 \pm 63)$ -2.95 (-1.04)	$-689 \pm 162 (-289 \pm 75)$ -11.47 (-4.81)	$-602 \pm 139 (-303 \pm 82)$ -10.04 (-5.05)	$-385 \pm 60$	$-416 \pm 64$
A10Kin energy/lipid	$-628 \pm 108 \ (-123 \pm 55)$ $-2.61 \ (-0.51)$	$-622 \pm 99 (-132 \pm 53)$ -2.59 (-0.55)	$-388 \pm 113 \ (-134 \pm 66)$ $-6.5 \ (-2.2)$	$-453 \pm 104 (-148 \pm 56)$ -7.55 (-2.46)	$-1262 \pm 111$	$-1275 \pm 75$
"The values in parentheses are for K28 only.						

A10Kin because in this barrel the K28 point toward the pore lumen.

Interactions between the peptides is another factor that plays a role in stabilizing the structure of the barrels. The interpeptide energy is more negative in the A10kin barrel than the P10Kout barrel (Table 2). This is clearly because the A10Kin barrel maintains a more compact structure with more extensive

contacts between neighboring peptide strands, whereas the P10Kout barrel deviates from its initial barrel-like structure as its N-terminal end extends into the water phase and becomes disordered. The distance between the peptides in the P10Kout barrel also tends to fluctuate and is usually larger than in the A10kin barrel. As a result, the diameter of the membrane pore created by the P10Kout barrel is also larger.

**Pore Hydration.** The hydration level of the pore lumen was examined to elucidate the possibility of ion conduction. Dehydrated gaps are observed at the center of the pores for both barrels over the course of the trajectories. In the case of the A10Kin barrel, water starts to leave the pore around 300 ns into the trajectory. The pore remains dehydrated for most of the simulation time thereafter, with water molecules occasionally entering the pore lumen. This dehydrated gap is about 11 Å in thickness and usually spans the length of six nonpolar residues starting with Lys28 and ending with Gly33, although a continuous water wire is seen around 1.3-1.4 µs and after the break in the barrel around 7.5  $\mu$ s. The thickness of the dehydrated gap is smaller in the case of the P10Kout barrel, usually spanning 4 amino acid residues from Ala30 to Gly33. Moreover, in the case of P10Kout, water is seen entering the pore and creating a continuous water wire more frequently than in the case of the A10kin barrel. Therefore, the thickness of the dehydrated gap tends to fluctuate at about 8-9 Å.

To confirm these observations, the length of the two barrels was divided into four slabs and the number of water molecules in each slab was obtained for each frame of the trajectory and averaged over all frames. In both cases, the two slabs corresponding to the terminal regions of the pore had the highest number of water molecules. The number of water molecules then decreased significantly for the two slabs at the center of the pore (Table 3). The numbers of chloride and

Table 3. Number of Water Molecules and Ions in Slabs Parallel to the Membrane<sup>a</sup>

systems		slab 1	slab 2	slab 3	slab 4
P10kout	amino acid	M35	I32	I32, I31	N27, S26
	water	76.9	3.9	26.8	135.8
	Cl <sup>-</sup>	0.18	0	0	0.02
	K <sup>+</sup>	0.15	0	1.68	6.53
A10kin	amino acid	K28, L34	I32	I32, A30	K28, L34
	water	76.9	4.5	16.3	110.1
	Cl <sup>-</sup>	0.49	0	0	0.14
	K <sup>+</sup>	0.42	0	0	0.49

<sup>&</sup>lt;sup>a</sup>The residues that line the pore in that slab are also shown.

potassium ions in the pore lumen were also calculated using a similar approach. Occasionally chloride approaches the Lys from the aqueous phase, but for both barrels, the center of the pore is

devoid of any ions. We have not seen any ion crossing the channels.

**Effect of Voltage.** The final structures from the 10  $\mu$ s trajectories were subjected to a further 10 ns of all-atom simulation in the presence of an electric field corresponding to a voltage drop of  $\pm 0.5$  V. These simulations were carried out with the Efield facility of the NAMD package. The A10kin structure is symmetric across the membrane, so the direction of the voltage should make no difference in the results. The dehydrated gap persisted, and no ion crossing was observed. A few Cl<sup>-</sup> ions were seen to approach the channel and interact with the K28 side chains. For the P10kout model, the direction of the voltage had a large impact on the structure (Figure 4). When the voltage was negative on the N-terminal side, the structure was stable. A few K<sup>+</sup> are seen interacting with the C-termini, and a few Cl<sup>-</sup> interact with the K28. However, the dehydrated gap persisted and no ions crossed the channel. When the voltage was positive on the N-terminal side, the Lysines were pulled toward the C-terminal side and the barrel structure broke apart (Figure 4). This is consistent with the experimental observation that ion channels were formed only with trans negative voltage. 17

#### DISCUSSION

This work explores possible mechanisms of membrane pore formation by Ab25-35. We tried to identify membraneembedded structures that are kinetically stable on the multimicrosecond time scale. To our knowledge, these are the longest simulations yet of this peptide. Nevertheless, this time scale is still very short by experimental standards, and because we start from preformed, membrane-embedded structures, we cannot ascertain that these structures are thermodynamically stable. They correspond to local free energy minima, whose height relative to other states is unknown. Unfortunately, we do not have a method of estimating the relative free energy of such complex peptide-lipid systems. The implicit membrane method gives approximate estimates of free energies, but these do not include the entropic cost of bringing peptides together in a precise configuration and the membrane deformation free energy. These putative structures can only point to possibilities that should be validated by independent means.

The structures presented here are more ordered and symmetric than structures of oligomers obtained by simulations in solution. This discrepancy results primarily from the difference in starting structures and the short time scale of the

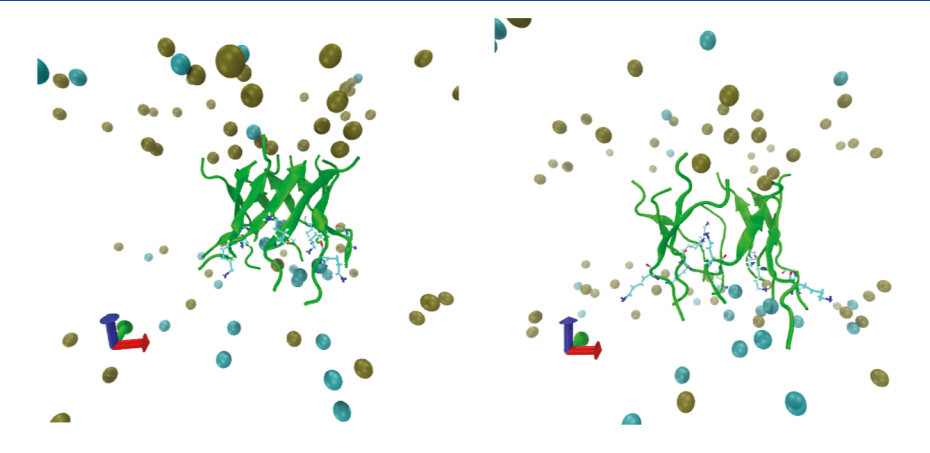


Figure 4. P10Kout after 10 ns of MD in the presence of voltage. Negative down (left) and negative up (right). K<sup>+</sup> ions are shown in tan color, and Cl<sup>-</sup> ions are shown in cyan color. Water and lipids are not shown for clarity.

simulations and possibly also from the different environment (polar vs nonpolar). The true amount of order present in experimentally studied amyloid oligomers is unknown. Another difficulty in computational work is the slow kinetics of membrane insertion. Experimental studies incubate for hours before they see beta-sheet-rich structures stabilized in lipid vesicles<sup>20</sup> and ion channel opening takes minutes. <sup>18</sup> These time scales are far removed from those available to the computational community. The oligomeric state also affects the propensity to insert into membranes. <sup>62</sup> Monomers and dimers <sup>63</sup> are less likely to insert than higher oligomers.

It has been argued that multiple short trajectories are better than a single long trajectory, like those presented here. However, this depends on the question being asked. If one aims to thoroughly characterize a well-established native state  $^{64}$  or a disordered system,  $^{62,65}$  multiple shorter simulations seem preferable. However, if one wants to see if a pore collapses and this collapse takes, say, 10  $\mu s$ , doing 100 simulations of 100 ns each will not be useful. The multiple short simulations will exhaustively sample a high-free energy state that is not really of interest.

Various types of experimental data could be examined for agreement or disagreement with the structural models. For example, electrophysiology experiments found ion channels that are weakly cation-selective, 17 which seems to disfavor A10Kin, which has K28 at the pore entrances. The channels were found to be blocked by Cu(II) and Cd(II). This could have been explained by the presence of Met35 in the pore lumen of P10Kout, except that Met is known to bind Cu(I), not Cu(II). 66,67 The finding of EPR studies that the N-terminal region of the peptide is in solution<sup>25</sup> seems more consistent with the P10Kout structure, where all the K28 are on the same side interacting with lipid phosphates. The fact that ion channel activity was observed only with negative voltage <sup>17</sup> also seems to support the P10Kout structure. A symmetric structure like A10Kin is incompatible with such an asymmetric voltage dependence. The brief runs under voltage show the P10Kout channel to be stable when the voltage is negative on the side of the K28 side chains. The reverse voltage pushes K28 toward the other side and that destabilizes the channel. In principle, reverse voltage would stabilize the reverse channel orientation, but the kinetics of the flipping process may be slow. Kinetics could also play a role in the experimental setup, where the peptides are placed on one side of the membrane and either the N-terminus or the C-terminus has to cross the membrane to establish a pore. Basic side chains and positive charges appear to cross membranes more easily than acidic side chains and negative charges. <sup>68–70</sup>

The single-channel conductance of Ab2535 channels in 100 mM NaCl exhibits wide heterogeneity, from 8 to 600 pS. <sup>18</sup> The heterogeneity could be due to different oligomeric states. At 0.5 V, these conductances would correspond to crossing times of 0.5–40 ns. Our long simulations without voltage and brief preliminary simulations under voltage did not show ion permeation. The dehydrated areas in the two channels provide a barrier to ion movement; this mechanism of preventing ion flow is known as hydrophobic gating. <sup>71–73</sup> However, the presence of voltage favors wetting of the pore and ion conduction. <sup>74</sup> Thus, the studies under voltage should be extended and expanded by considering, for example, the effects of replacing K<sup>+</sup> with Na<sup>+</sup> or Ca<sup>2+</sup> and calculating free energy profiles for ion permeation. Different oligomeric states should also be considered.

The effects of numerous mutations on aggregation and toxicity have been measured. State 15. It would be useful to examine them in the context of the current pore structures. Some studies found M35 to be critical for Ab25-35 toxicity. For example, mutation of M35 to Cys or Ser maintained toxicity, Asp reduced it somewhat, and Lys, Leu, Tyr, and Norleucine abrogated it. However, other studies with different sample preparation protocols found that M35V and M35norL were equally toxic. M35A made the peptide more toxic, and lengthening the peptide by adding residue 36 made it either less toxic or nontoxic. The A10Kin structure, where Met is toward the membrane, cannot explain the effect of these mutations. In the P10Kout structure, half of the M35 are in the pore lumen and the rest, due to crowding and the register shift, move toward the solution (Figure 5). Replacement of M35 by smaller residues

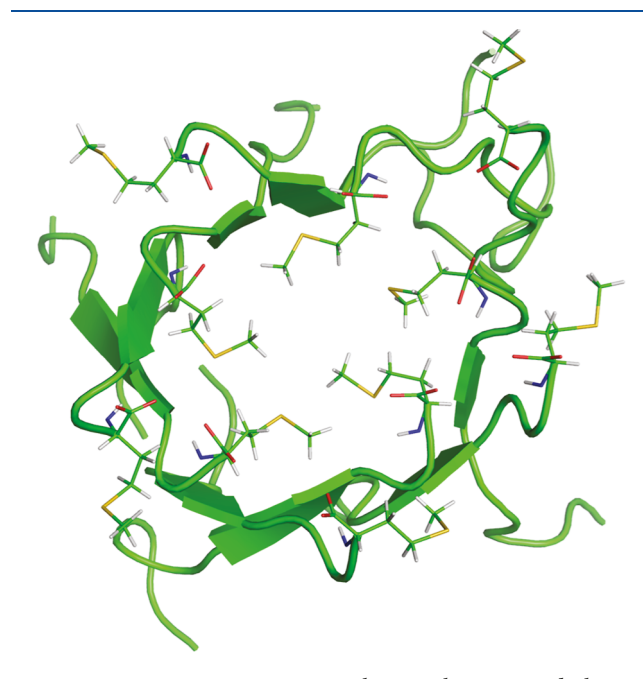


**Figure 5.** P10Kout at 5  $\mu$ s, top view, showing the Met35 sidechains.

should in principle increase ion conduction. Replacement by larger residues could destabilize the structure due to clashes unless the oligomeric number increased, with higher entropic cost. Adding residue 36 could hamper the movement of half of the M35 away from the pore lumen, exacerbating the clashes. Thus, some mutations can be explained by the P10Kout structure. However, others cannot. For example, N27A was found to be less toxic. To In the P10Kout structure, N27 is in the disordered N-terminal region and it is hard to see why it would have such an effect. Perhaps it lowers the tendency of the peptide to oligomerize, which is a step upstream of pore formation. Results on even shorter fragments differ. Older studies found the 31-35 fragment to be inactive, but more recent ones found it to be toxic. The These are exactly the residues involved in the short barrel of our P10Kout structure.

In much of the literature, the 25-35 fragment has been thought of as a proxy for the full-length peptide because it recapitulates its main properties, i.e., fibrilization and toxicity. There has been some evidence, however, that they may work via different mechanisms. Could these pore structures be formed by the full-length peptide, with the rest of the peptide disordered near the membrane? The antiparallel structure would put the bulk of the peptide on different sides of the membrane. That might be

possible if the peptide were preincorporated within the lipids but very difficult for an oligomer approaching an already formed cell membrane, as in the situation in vivo. The parallel structure would be more likely, although the presence of the hydrophobic 36–42 residues would complicate the situation. As mentioned above, addition of residue 36 reduces or eliminates the toxicity. To our knowledge, no toxicity measurements have been done for 25–40 or 25–42. In previous work, we considered pore structures formed by the full-length peptide and found that the hydrophobic tail alone is unable to support an aqueous pore. <sup>56</sup>

Whether the 25-35 fragment is physiologically relevant in Alzheimer's disease is debatable. Although it has been found in Alzheimer's patients' brains, <sup>13</sup> no other evidence supports its involvement in the disease. However, it is a small model system showing cytotoxicity and ion channel formation, and it would be worth understanding in detail. This can only be achieved with further experimentation together with additional computational studies

#### ASSOCIATED CONTENT

#### **Supporting Information**

The Supporting Information is available free of charge at https://pubs.acs.org/doi/10.1021/acs.biochem.3c00323.

Additional figures of the final structures of the all-atom simulations for the antiparallel and parallel barrel decamers (PDF)

Final structure of the all-atom simulations for the antiparallel barrel decamer (PDB)

Final structure of the all-atom simulations for the parallel barrel decamer (PDB)

#### AUTHOR INFORMATION

#### **Corresponding Author**

Themis Lazaridis — Department of Chemistry, City College of New York/CUNY, New York, New York 10031, United States; Graduate Programs in Chemistry, Biochemistry, and Physics The Graduate Center, City University of New York, New York, New York 10016, United States; orcid.org/0000-0003-4218-7590; Phone: (212) 650-8364; Email: tlazaridis@ccny.cuny.edu

#### **Authors**

Ankita Dutta — Department of Chemistry, City College of New York/CUNY, New York, New York 10031, United States; Graduate Program in Biochemistry, The Graduate Center, City University of New York, New York, New York 10016, United States

Aliasghar Sepehri – Department of Chemistry, City College of New York/CUNY, New York, New York 10031, United States

Complete contact information is available at: https://pubs.acs.org/10.1021/acs.biochem.3c00323

#### Notes

The authors declare no competing financial interest.

#### ACKNOWLEDGMENTS

This work was supported by the National Science Foundation (MCB-1855942). Anton computer time was provided by the Pittsburgh Supercomputing Center through grant R01GM116961 from the NIH. The Anton machine at the PSC was generously made available by D.E. Shaw. Research and computer time was provided by the National Center for

Multiscale Modeling of Biological Systems through grant number P41GM103712-S1 from the NIH and the Pittsburgh Supercomputing Center. We thank Dr. Suren A. Tatulian for helpful comments.

#### REFERENCES

- (1) Hardy, J.; Allsop, D. Amyloid Deposition as the Central Event in the Aetiology of Alzheimer's Disease. *Trends Pharmacol. Sci.* **1991**, *12*, 383–388.
- (2) Millucci, L.; Ghezzi, L.; Bernardini, G.; Santucci, A. Conformations and Biological Activities of Amyloid Beta Peptide 25-35. *Curr. Protein Pept. Sci.* **2010**, *11*, 54–67.
- (3) Kaminsky, Y. G.; Marlatt, M. W.; Smith, M. A.; Kosenko, E. A. Subcellular and Metabolic Examination of Amyloid- $\beta$  Peptides in Alzheimer Disease Pathogenesis: Evidence for A $\beta$ 25-35. *Exp. Neurol.* **2010**, 221, 26–37.
- (4) Pike, C. J.; Burdick, D.; Walencewicz, A. J.; Glabe, C. G.; Cotman, C. W. Neurodegeneration Induced by  $\beta$ -Amyloid Peptides in Vitro: The Role of Peptide Assembly State. *J. Neurosci.* **1993**, *13*, 1676–1687.
- (5) Pike, C. J.; Walencewicz-Wasserman, A. J.; Kosmoski, J.; Cribbs, D. H.; Glabe, C. G.; Cotman, C. W. Structure-Activity Analyses of  $\beta$ -Amyloid Peptides: Contributions of the B25-35 Region to Aggregation and Neurotoxicity. *J. Neurochem.* **2002**, *64*, 253–265.
- (6) Mattson, M. P.; Cheng, B.; Davis, D.; Bryant, K.; Lieberburg, I.; Rydel, R. E. beta-Amyloid peptides destabilize calcium homeostasis and render human cortical neurons vulnerable to excitotoxicity. *J. Neurosci.* **1992**, *12*, 376–389.
- (7) Furukawa, K.; Abe, Y.; Akaike, N. Amyloid  $\beta$  Protein-Induced Irreversible Current in Rat Cortical Neurones. *Neuroreport* **1994**, *5*, 2016–2018.
- (8) Simmons, M. A.; Schneider, C. R. Amyloid  $\beta$  Peptides Act Directly on Single Neurons. *Neurosci. Lett.* **1993**, *150*, 133–136.
- (9) Oyama, Y.; Chikahisa, L.; Ueha, T.; Hatakeyama, Y.; Kokubun, T. Change in Membrane Permeability Induced by Amyloid  $\beta$ -Protein Fragment 25-35 in Brain Neurons Dissociated from Rats. *Jpn. J. Pharmacol.* **1995**, *68*, 77–83.
- (10) Loo, D. T.; Copani, A.; Pike, C. J.; Whittemore, E. R.; Walencewicz, A. J.; Cotman, C. W. Apoptosis Is Induced by  $\beta$ -Amyloid in Cultured Central Nervous System Neurons. *Proc. Natl. Acad. Sci. U.S.A.* **1993**, *90*, 7951–7955.
- (11) Clementi, M. E.; Marini, S.; Coletta, M.; Orsini, F.; Giardina, B.; Misiti, F.  $A\beta(31\text{-}35)$  and  $A\beta(25\text{-}35)$  Fragments of Amyloid Beta-Protein Induce Cellular Death through Apoptotic Signals: Role of the Redox State of Methionine-35. *FEBS Lett.* **2005**, *579*, 2913–2918.
- (12) Mattson, M. P.; Begley, J. G.; Mark, R. J.; Furukawa, K. A $\beta$ 25-35 Induces Rapid Lysis of Red Blood Cells: Contrast with A $\beta$ 1-42 and Examination of Underlying Mechanisms. *Brain Res.* **1997**, 771, 147–153
- (13) Kubo, T.; Nishimura, S.; Kumagae, Y.; Kaneko, I. In Vivo Conversion of Racemized Bamyloid ([D-Ser26]Aβ1-40) to Truncated and Toxic Fragments ([D-Ser26]Aβ25-35/40) and Fragment Presence in the Brains of Alzheimer's Patients. *J. Neurosci. Res.* **2002**, 70, 474–483
- (14) Näslund, J.; Schierhorn, A.; Hellman, U.; Lannfelt, L.; Roses, A. D.; Tjernberg, L. O.; Silberring, J.; Gandy, S. E.; Winblad, B.; Greengard, P.; et al. Relative Abundance of Alzheimer A $\beta$  Amyloid Peptide Variants in Alzheimer Disease and Normal Aging. *Proc. Natl. Acad. Sci. U.S.A.* **1994**, *91*, 8378–8382.
- (15) Maddalena, A. S.; Papassotiropoulos, A.; Gonzalez-Agosti, C.; Signorell, A.; Hegi, T.; Pasch, T.; Nitsch, R. M.; Hock, C. Cerebrospinal Fluid Profile of Amyloid  $\beta$  Peptides in Patients with Alzheimer's Disease Determined by Protein Biochip Technology. *Neurodegener. Dis.* **2004**, *1*, 231–235.
- (16) Wildburger, N. C.; Esparza, T. J.; Leduc, R. D.; Fellers, R. T.; Thomas, P. M.; Cairns, N. J.; Kelleher, N. L.; Bateman, R. J.; Brody, D. L. Diversity of Amyloid-Beta Proteoforms in the Alzheimer's Disease Brain. *Sci. Rep.* **2017**, *7*, 9520.

- (17) Mirzabekov, T.; Lin, M. C.; Yuan, W. L.; Marshall, P. J.; Carman, M.; Tomaselli, K.; Lieberburg, I.; Kagan, B. L. Channel Formation in Planar Lipid Bilayers by a Neurotoxic Fragment of the  $\beta$ -Amyloid Peptide. *Biochem. Biophys. Res. Commun.* **1994**, 202, 1142–1148.
- (18) Lin, M. C. A.; Kagan, B. L. Electrophysiologic Properties of Channels Induced by A $\beta$ 25-35 in Planar Lipid Bilayers. *Peptides* **2002**, 23, 1215–1228.
- (19) Kandel, N.; Zheng, T.; Huo, Q.; Tatulian, S. A. Membrane Binding and Pore Formation by a Cytotoxic Fragment of Amyloid  $\beta$  Peptide. *J. Phys. Chem. B* **2017**, *121*, 10293–10305.
- (20) Kandel, N.; Matos, J. O.; Tatulian, S. A. Structure of Amyloid  $\beta$  25–35 in Lipid Environment and Cholesterol-Dependent Membrane Pore Formation. *Sci. Rep.* **2019**, *9*, 2689.
- (21) Terzi, E.; Hoelzemann, G.; Seelig, J. Alzheimer .beta.-Amyloid Peptide 25-35: Electrostatic Interactions with Phospholipid Membranes. *Biochemistry* **1994**, 33, 7434–7441.
- (22) Mason, R. P.; Estermyer, J. D.; Kelly, J. F.; Mason, P. E. Alzheimer's Disease Amyloid  $\beta$  Peptide 25-35 Is Localized in the Membrane Hydrocarbon Core: X-Ray Diffraction Analysis. *Biochem. Biophys. Res. Commun.* **1996**, 222, 78–82.
- (23) Dante, S.; Hauss, T.; Dencher, N. A. B-Amyloid 25 To 35 Is Intercalated in Anionic and Zwitterionic Lipid Membranes To Different Extents. *Biophys. J.* **2002**, *83*, 2610–2616.
- (24) Dante, S.; Hauss, T.; Dencher, N. A. Insertion of Externally Administered Amyloid  $\beta$  Peptide 25-35 and Perturbation of Lipid Bilayers. *Biochemistry* **2003**, 42, 13667–13672.
- (25) Esposito, C.; Tedeschi, A.; Scrima, M.; D'Errico, G.; Ottaviani, M. F.; Rovero, P.; D'Ursi, A. M. Exploring Interaction of  $\beta$ -Amyloid Segment (25–35) with Membrane Models through Paramagnetic Probes. *J. Pept. Sci.* **2006**, *12*, 766–774.
- (26) Lau, T. L.; Gehman, J. D.; Wade, J. D.; Perez, K.; Masters, C. L.; Barnham, K. J.; Separovic, F. Membrane Interactions and the Effect of Metal Ions of the Amyloidogenic Fragment  $A\beta$ (25-35) in Comparison to  $A\beta$ (1-42). *Biochim. Biophys. Acta, Biomembr.* **2007**, 1768, 2400–2408.
- (27) D'Errico, G.; Vitiello, G.; Ortona, O.; Tedeschi, A.; Ramunno, A.; D'Ursi, A. M. Interaction between Alzheimer's  $A\beta$ (25-35) Peptide and Phospholipid Bilayers: The Role of Cholesterol. *Biochim. Biophys. Acta, Biomembr.* **2008**, *1778*, 2710–2716.
- (28) Kohno, T.; Kobayashi, K.; Maeda, T.; Sato, K.; Takashima, A. Three-Dimensional Structures of the Amyloid  $\beta$  Peptide (25-35) in Membrane-Mimicking Environment. *Biochemistry* **1996**, 35, 16094–16104
- (29) D'Ursi, A. M.; Armenante, M. R.; Guerrini, R.; Salvadori, S.; Sorrentino, G.; Picone, D. Solution Structure of Amyloid  $\beta$ -Peptide (25-35) in Different Media. *J. Med. Chem.* **2004**, *47*, 4231–4238.
- (30) Terzi, E.; Hoelzemann, G.; Seelig, J. Reversible Random Coil-.beta.-Sheet Transition of the Alzheimer .beta.-Amyloid Fragment (25-35). *Biochemistry* **1994**, *33*, 1345–1350.
- (31) Shanmugam, G.; Polavarapu, P. L. Structure of  $A\beta$ (25-35) Peptide in Different Environments. *Biophys. J.* **2004**, 87, 622–630.
- (32) Wei, G.; Shea, J. E. Effects of Solvent on the Structure of the Alzheimer Amyloid- $\beta$ (25-35) Peptide. *Biophys. J.* **2006**, *91*, 1638–1647.
- (33) Tsai, H. H. G.; Lee, J. B.; Tseng, S. S.; Pan, X. A.; Shih, Y. C. Folding and Membrane Insertion of Amyloid-Beta (25-35) Peptide and Its Mutants: Implications for Aggregation and Neurotoxicity. *Proteins: Struct., Funct., Bioinf.* **2010**, 78, 1909–1925.
- (34) Tsai, H. H. G.; Lee, J. B.; Shih, Y. C.; Wan, L.; Shieh, F. K.; Chen, C. Y. Location and Conformation of Amyloid  $\beta$ (25-35) Peptide and Its Sequence-Shuffled Peptides within Membranes: Implications for Aggregation and Toxicity in PC12 Cells. *ChemMedChem* **2014**, *9*, 1002–1011.
- (35) Smith, A. K.; Klimov, D. K. Binding of Cytotoxic A $\beta$ 25-35 Peptide to the Dimyristoylphosphatidylcholine Lipid Bilayer. *J. Chem. Inf. Model.* **2018**, 58, 1053–1065.
- (36) Smith, A. K.; Klimov, D. K. De Novo Aggregation of Alzheimer's  $A\beta$ 25-35 Peptides in a Lipid Bilayer. *Sci. Rep.* **2019**, *9*, 7161.

- (37) Smith, A. K.; Khayat, E.; Lockhart, C.; Klimov, D. K. Do Cholesterol and Sphingomyelin Change the Mechanism of A $\beta$ 25-35 Peptide Binding to Zwitterionic Bilayer? *J. Chem. Inf. Model.* **2019**, 59, 5207–5217.
- (38) Fu, Z.; Luo, Y.; Derreumaux, P.; Wei, G. Induced β-Barrel Formation of the Alzheimer's Aβ25-35 Oligomers on Carbon Nanotube Surfaces: Implication for Amyloid Fibril Inhibition. *Biophys. J.* **2009**, *97*, 1795–1803.
- (39) Chang, Z.; Luo, Y.; Zhang, Y.; Wei, G. Interactions of Aβ25-35 β-Barrel-like Oligomers with Anionic Lipid Bilayer and Resulting Membrane Leakage: An All-Atom Molecular Dynamics Study. J. Phys. Chem. B 2011, 115, 1165–1174.
- (40) Colletier, J. P.; Laganowsky, A.; Landau, M.; Zhao, M.; Soriaga, A. B.; Goldschmidt, L.; Flot, D.; Cascio, D.; Sawaya, M. R.; Eisenberg, D. Molecular Basis for Amyloid- $\beta$  Polymorphism. *Proc. Natl. Acad. Sci. U.S.A.* **2011**, *108*, 16938–16943.
- (41) Neria, E.; Fischer, S.; Karplus, M. Simulation of Activation Free Energies in Molecular Systems. *J. Chem. Phys.* **1996**, *105*, 1902–1921.
- (42) Lazaridis, T.; Karplus, M. Effective Energy Function for Proteins in Solution. *Proteins: Struct., Funct., Bioinf.* **1999**, *35*, 133–152.
- (43) Lazaridis, T. Effective Energy Function for Proteins in Lipid Membranes. *Proteins: Struct., Funct., Bioinf.* **2003**, *52*, 176–192.
- (44) Lazaridis, T. Structural Determinants of Transmembrane Beta-Barrels. *J. Chem. Theory Comput.* **2005**, *1*, 716–722.
- (45) Mihajlovic, M.; Lazaridis, T. Antimicrobial Peptides Bind More Strongly to Membrane Pores. *Biochim. Biophys. Acta, Biomembr.* **2010**, 1798, 1494–1502.
- (46) Lazaridis, T. Implicit Solvent Simulations of Peptide Interactions with Anionic Lipid Membranes. *Proteins: Struct., Funct., Bioinf.* **2004**, 58, 518–527.
- (47) Brooks, B. R.; Brooks, C. L., 3rd; Mackerell, A. D., Jr.; Nilsson, L.; Petrella, R. J.; Roux, B.; Won, Y.; Archontis, G.; Bartels, C.; Boresch, S.; et al. CHARMM: The Biomolecular Simulation Program. *J. Comput. Chem.* **2009**, *30*, 1545–1614.
- (48) He, Y.; Prieto, L.; Lazaridis, T. Modeling Peptide Binding to Anionic Membrane Pores. *J. Comput. Chem.* **2013**, *34*, 1463–1475.
- (49) He, Y.; Lazaridis, T. Activity Determinants of Helical Antimicrobial Peptides: A Large-Scale Computational Study. *PLoS One* **2013**, *8*, No. e66440.
- (50) Rahaman, A.; Lazaridis, T. A thermodynamic approach to alamethicin pore formation. *Biochim. Biophys. Acta, Biomembr.* **2014**, 1838, 1440–1447.
- (51) Lipkin, R.; Pino-Angeles, A.; Lazaridis, T. Transmembrane Pore Structures of  $\beta$ -Hairpin Antimicrobial Peptides by All-Atom Simulations. *J. Phys. Chem. B* **2017**, *121*, 9126–9140.
- (52) Lipkin, R.; Lazaridis, T. Computational Prediction of the Optimal Oligomeric State for Membrane-Inserted  $\beta$ -Barrels of Protegrin-1 and Related Mutants. *J. Pept. Sci.* **2017**, 23, 334–345.
- (53) Lipkin, R. B.; Lazaridis, T. Implicit Membrane Investigation of the Stability of Antimicrobial Peptide  $\beta$ -Barrels and Arcs. *J. Membr. Biol.* **2015**, 248, 469–486.
- (54) Lazaridis, T.; He, Y.; Prieto, L. Membrane Interactions and Pore Formation by the Antimicrobial Peptide Protegrin. *Biophys. J.* **2013**, *104*, 633–642.
- (55) Sepehri, A.; Nepal, B.; Lazaridis, T. Distinct Modes of Action of IAPP Oligomers on Membranes. *J. Chem. Inf. Model.* **2021**, *61*, 4645–4655.
- (56) Sepehri, A.; Lazaridis, T. Putative Structures of Membrane-Embedded Amyloid  $\beta$  Oligomers. ACS Chem. Neurosci. **2023**, 14, 99–110.
- (57) Maurer, M.; Lazaridis, T. Transmembrane  $\beta$ -Barrel Models of  $\alpha$ -Synuclein Oligomers, **2023**. submitted.
- (58) Best, R. B.; Zhu, X.; Shim, J.; Lopes, P. E. M.; Mittal, J.; Feig, M.; MacKerell, A. D. Optimization of the Additive CHARMM All-Atom Protein Force Field Targeting Improved Sampling of the Backbone  $\varphi$ ,  $\psi$  and Side-Chain X1 and X2 Dihedral Angles. *J. Chem. Theory Comput.* **2012**, *8*, 3257–3273.
- (59) Klauda, J. B.; Venable, R. M.; Freites, J. A.; O'Connor, J. W.; Tobias, D. J.; Mondragon-Ramirez, C.; Vorobyov, I.; MacKerell, A. D.,

- Jr.; Pastor, R. W. Update of the CHARMM All-Atom Additive Force Field for Lipids: Validation on Six Lipid Types. *J. Phys. Chem. B* **2010**, 114, 7830–7843.
- (60) Shaw, D. E.; Grossman, J. P.; Bank, J. A.; Batson, B.; Butts, J. A.; Chao, J. C.; Deneroff, M. M.; Dror, R. O.; Even, A.; Fenton, C. H.; et al. Anton 2: Raising the Bar for Performance and Programmability in a Special-Purpose Molecular Dynamics Supercomputer. SC '14: Proceedings of the International Conference for High Performance Computing, Networking, Storage and Analysis, 2014; pp 41–53.
- (61) Voelker, M. J.; Barz, B.; Urbanc, B. Fully Atomistic Aβ40 and Aβ42 Oligomers in Water: Observation of Porelike Conformations. *J. Chem. Theory Comput.* **2017**, *13*, 4567–4583.
- (62) Andrews, B.; Ruggiero, T.; Urbanc, B. How Do Salt and Lipids Affect Conformational Dynamics of  $A\beta$ 42 Monomers in Water? *Phys. Chem. Chem. Phys.* **2023**, 25, 2566–2583.
- (63) Fatafta, H.; Khaled, M.; Owen, M. C.; Sayyed-Ahmad, A.; Strodel, B. Amyloid- $\beta$  Peptide Dimers Undergo a Random Coil to  $\beta$ -Sheet Transition in the Aqueous Phase but Not at the Neuronal Membrane. *Proc. Natl. Acad. Sci. U.S.A.* **2021**, *118*, No. e2106210118.
- (64) Caves, L. S. D.; Evanseck, J. D.; Karplus, M. Locally Accessible Conformations of Proteins: Multiple Molecular Dynamics Simulations of Crambin. *Protein Sci.* **1998**, *7*, 649–666.
- (65) Knapp, B.; Ospina, L.; Deane, C. M. Avoiding False Positive Conclusions in Molecular Simulation: The Importance of Replicas. *J. Chem. Theory Comput.* **2018**, *14*, 6127–6138.
- (66) Rubino, J. T.; Riggs-Gelasco, P.; Franz, K. J. Methionine Motifs of Copper Transport Proteins Provide General and Flexible Thioether-Only Binding Sites for Cu(I) and Ag(I). *J. Biol. Inorg. Chem.* **2010**, *15*, 1033–1049.
- (67) Shenberger, Y.; Marciano, O.; Gottlieb, H. E.; Ruthstein, S. Insights into the N-Terminal Cu(II) and Cu(I) Binding Sites of the Human Copper Transporter CTR1. *J. Coord. Chem.* **2018**, *71*, 1985–2002.
- (68) Marks, J. R.; Placone, J.; Hristova, K.; Wimley, W. C. Spontaneous Membrane-Translocating Peptides by Orthogonal High-Throughput Screening. *J. Am. Chem. Soc.* **2011**, *133*, 8995–9004.
- (69) Cardenas, A. E.; Shrestha, R.; Webb, L. J.; Elber, R. Membrane Permeation of a Peptide: It Is Better to Be Positive. *J. Phys. Chem. B* **2015**, *119*, 6412–6420.
- (70) Sani, M. A.; Separovic, F. How Membrane-Active Peptides Get into Lipid Membranes. *Acc. Chem. Res.* **2016**, *49*, 1130–1138.
- (71) Beckstein, O.; Biggin, P. C.; Sansom, M. S. P. A Hydrophobic Gating Mechanism for Nanopores. *J. Phys. Chem. B* **2001**, *105*, 12902–12905.
- (72) Anishkin, A.; Sukharev, S. Water Dynamics and Dewetting Transitions in the Small Mechanosensitive Channel MscS. *Biophys. J.* **2004**, *86*, 2883–2895.
- (73) Zhu, F.; Hummer, G. Pore Opening and Closing of a Pentameric Ligand-Gated Ion Channel. *Proc. Natl. Acad. Sci. U.S.A.* **2010**, *107*, 19814—19819.
- (74) Spronk, S. A.; Elmore, D. E.; Dougherty, D. A. Voltage-Dependent Hydration and Conduction Properties of the Hydrophobic Pore of the Mechanosensitive Channel of Small Conductance. *Biophys. J.* **2006**, *90*, 3555–3569.
- (75) Sato, K.; Wakamiya, A.; Maeda, T.; Noguchi, K.; Takashima, A.; Imahori, K. Correlation among Secondary Structure, Amyloid Precursor Protein Accumulation, and Neurotoxicity of Amyloid  $\beta$ (25-35) Peptide as Analyzed by Single Alanine Substitution. *J. Biochem.* **1995**, *118*, 1108–1111.
- (76) Varadarajan, S.; Kanski, J.; Aksenova, M.; Lauderback, C.; Butterfield, D. A. Different Mechanisms of Oxidative Stress and Neurotoxicity for Alzheimer's  $A\beta(1-42)$  and  $A\beta(25-35)$ . *J. Am. Chem. Soc.* **2001**, *123*, 5625–5631.
- (77) Maiti, P.; Lomakin, A.; Benedek, G. B.; Bitan, G. Despite Its Role in Assembly, Methionine 35 Is Not Necessary for Amyloid  $\beta$ -Protein Toxicity. *J. Neurochem.* **2010**, *113*, 1252–1262.
- (78) Yan, X. Z.; Qiao, J. T.; Dou, Y.; Qiao, Z. D.  $\beta$ -Amyloid Peptide Fragment 31-35 Induces Apoptosis in Cultured Cortical Neurons. *Neuroscience* **1999**, 92, 177–184.

### ☐ Recommended by ACS

## Pathways of hLL-37 $_{17.29}$ Aggregation Give Insight into the Mechanism of $\alpha$ -Amyloid Formation

Aritra Mitra and Sandip Paul

SEPTEMBER 14, 2023

THE JOURNAL OF PHYSICAL CHEMISTRY B

READ 🗹

### An S-Shaped A\(\beta\)42 Cross-\(\beta\) Hexamer Embedded into a Lipid Bilayer Reveals Membrane Disruption and Permeability

Phuong H Nguyen and Philippe Derreumaux

FEBRUARY 09, 2023

ACS CHEMICAL NEUROSCIENCE

READ 🗹

### Putative Structures of Membrane-Embedded Amyloid $\beta$ Oligomers

Aliasghar Sepehri and Themis Lazaridis

DECEMBER 16, 2022

ACS CHEMICAL NEUROSCIENCE

READ 🗹

# Lysine Acetylation Changes the Mechanism of A $\beta$ 25–35 Peptide Binding and Dimerization in the DMPC Bilayer

Elias Khayat, Dmitri K. Klimov, et al.

JANUARY 19, 2023

ACS CHEMICAL NEUROSCIENCE

READ **C** 

Get More Suggestions >